Journal of The Electrochemical Society

Nanostructured $LaFeO_3$ Photocathodes with Onset Potentials for the Hydrogen Evolution Reaction Over 1.4 V vs. RHE

Nanostructured $LaFeO_3$ Photocathodes with Onset Potentials for the Hydrogen Evolution Reaction Over 1.4 V vs. RHE

Xin Sun, Devendra Tiwari, and David J. Fermin *,z

School of Chemistry, University of Bristol, Canctocks Close, Bristol BS8 1TS, United Kingdom

The photoelectrochemical properties of phase-pure $LaFeO_3$ (LFO) nanostructured films are investigated upon modification with a thin TiO_2 film and Pt nanoparticles as a catalyst. $LaFeO_3$ with crystallite domains in the range of 60 nm are prepared by thermolysis of an ionic-liquid precursor and subsequently deposited onto FTO electrode by spin-coating. Deposition of a TiO_2 layer by solution-based methods leads to the formation of a heterojunction, attenuating dark current associated with hole-transfer (water oxidation) at potential above 1.4 V. The LFO/TiO_2 heterojunction features photocurrent onset potential for the hydrogen evolution reaction of 1.47 V vs. the reversible hydrogen electrode (RHE), which is one of the most positive values reported for a single absorber. Deposition of Pt nanoparticles at the LFO/TiO_2 heterostructure generates a significant increase in the HER photocurrent, although bulk recombination remains an important challenge in these constructs.
 [DOI: 10.1149/2.0141915jes]

Manuscript submitted July 22, 2019; revised manuscript received October 2, 2019. Published October 18, 2019.

The development of semiconductor electrodes capable of promoting unassisted water splitting is one of the grand challenges in electrochemical energy conversion.[1] Integrated III-V tandem absorber protected with thin oxide coatings have pushed solar-to-hydrogen efficiency to values in the range 14 to 16%,[2,3] re-injecting new momentum to the field. May et al. have shown that two-junction tandem absorber with GaInP *n-p* top cell and GaInAs *n-i-p* bottom cell can lead to photocurrent onset potentials for the hydrogen evolution reaction (HER) of 1.9 V vs. RHE.[4] This level of performance can make photoelectrochemical water-splitting competitive against electrolyzers powered by photovoltaic systems, although stability and costs remain significant hurdles. Stabilization of semiconductor surfaces by ultrathin TiO_2 layers deposited by atomic layer deposition (ALD)[5] has generated a strong impact in the field. This approach has been able to extend the stability of photoanodes by hundreds of hours under continuous illumination.[6] However, it is crucial to replicate the performance of III-V heterostructures with low-cost materials and scalable processing methods. Significant efforts have been devoted to so-called dimensionally stable photoelectrodes such as Fe_2O_3, WO_3 and $BiVO_4$.[7] The performance of these conventional oxides remain significantly below the target required for viable water-splitting technologies. Complex transition metal oxides comprise a vast family of compounds, as recently reviewed by Rajeshwar and co-workers.[8] Although materials in this space may hold the key to viable and scalable photoelectrochemical water-splitting technologies, our current knowledge on their structure-performance relationships remains very limited.

Transition metal oxides as photocathodes for the HER have been significantly less studied than photoanodes materials. Cu_2O remains the benchmark, showing external quantum efficiency (EQE) values as high as 76% and photocurrent onset potential of 0.48 V vs. RHE in the presence of a TiO_2 stabilization layer deposited by ALD.[9] Several ferrite photocathodes have been reported including $CaFe_2O_4$,[10] and $CuFeO_2$.[11] Celorrio et al. reported photovoltages as high as 1.2 V vs. RHE for the hydrogen evolution reaction at $LaFeO_3$ (LFO).[12] Other studies involving $LaFeO_3$[13–17] and $YFeO_3$[18] have also observed high photovoltages but EQE less than 1%. The origin of carrier losses remains to be fully elucidated.

In this work, we systematically investigate the photoelectrochemical properties of nanostructured LFO photocathodes by introducing a thin TiO_2 film as a hole-blocking layer and Pt nanoparticles as electrocatalysts. The fabrication of the photoactive constructs only involves solution-based methods. Our working hypothesis is that hole extraction (water oxidation) lead to majority carrier losses and low EQE values. Systematic analysis of the electrochemical responses as a function of the LFO modifications provides information about the band edge energy offset of the oxide, while generating a 10-fold increase in the photocurrent responses. We also achieved photocurrent onset potentials more positive than 1.4 V vs. RHE for the HER. To the best of our knowledge, this is the largest onset potential reported for a single absorber photocathode.

Experimental

LFO nanoparticles were prepared by employing a highly versatile ionic liquid-based precursor used for synthesizing a wide range of perovskite nanostructures.[12,18,19] As-prepared nanoparticles were dispersed in an ethanol solution (3.8% wt), containing ethyl cellulose (0.5% wt) and terpineol (36.0% wt). The nanoparticle suspension was spin-coated onto F:SnO_2 (FTO) films on glass. The films were heated at 500°C for 15 minutes after each coating step (2000 rpm for 30 seconds). TiO_2 films were prepared by spin-coating a solution composed of 11.2% titanium isopropoxide in 0.3% hydrochloric acid and 88.5% ethanol with a rotation speed of 4000 rpm for 60 seconds. The films were dried at 225°C for 5 minutes, followed by heating to 500°C for 30 minutes. Pt nanoparticles were prepared in aqueous solution by reducing by Na_2PtCl_4 (1 mM) in the presence of $NaBH_4$ (10 mM) and trisodium citrate (38.8 mM).[20] Pt nanoparticles were spin-coated (2000 rpm for 30 seconds), leading to a maximum Pt loading of 0.19 mg cm^{-2} for each deposition step. The films were subsequently heated at 400°C for 30 minutes, leading to the formation of Pt nanoparticles with an average crystallite size of 3 nm.

Photoelectrochemical experiments were carried out in Ar-purged aqueous solutions (Milli-Q systems 18.4 MΩ cm) containing 0.1 M Na_2SO_4 at pH 12. Illumination was provided by LEDs with different emission wavelengths (Thorlabs) driven by a waveform generator, while the power output was monitored by a calibrated Si photodiode. Current-voltage measurements were conducted with an Ivium Compactstat potentiostat, Ag/AgCl and glassy carbon rod as a reference electrode. All potentials are referred to against the reversible hydrogen electrode (RHE).

Results and Discussion

Figure 1A displays powder X-ray diffraction (XRD) patterns of LFO, TiO_2 and Pt nanoparticles which are indexed employing JCPDS-ICDD Files No. 01-075-0541, 01-086-1157 and 00-001-1194, respectively. LFO diffractogram is consistent with pure rhombohedral phase, while the LFO film topography in Figure 1B reveals grains with a mean size of 60 nm. The TiO_2 coating is composed of very small crystallites (anatase) with domain sizes of 7 nm as estimated from the broadening of the XRD features. The film morphology changes upon addition of

*Electrochemical Society Member.
zE-mail: david.fermin@bristol.ac.uk

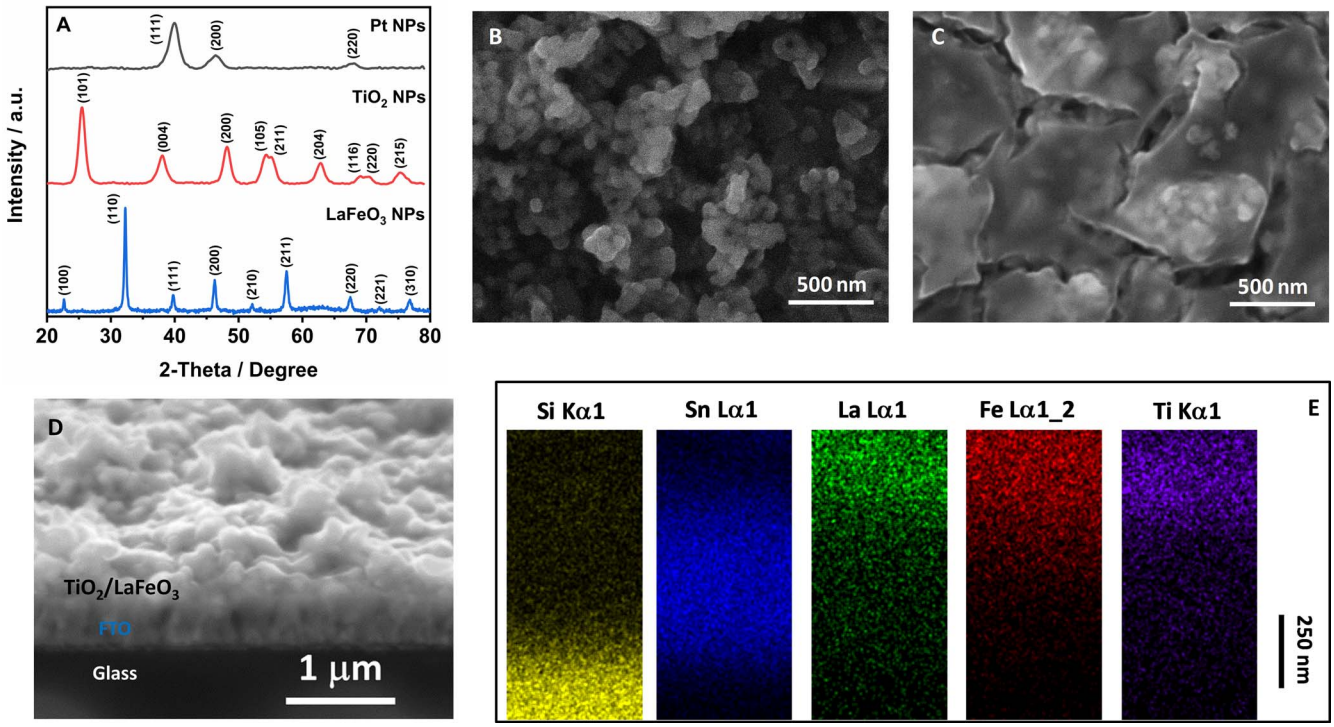

Figure 1. Structure and morphology of the LFO/TiO_2 photoelectrodes: XRD patterns of the LFO, TiO_2 and Pt nanoparticles (NPs), showing phase-pure nanoscale crystalline domains (A); top view SEM image of the LFO film prior (B) and after (C) TiO_2 deposition; cross-sectional SEM image (D) and EDX maps (E) of LFO/TiO_2 films revealing domains associated with FTO, LFO and TiO_2.

TiO_2 as shown in Figure 1C, revealing featureless coating over the LFO assembly. The SEM cross-section image in Figure 1D reveals a compact film with a highly corrugated surface and little contrast between the LFO and TiO_2 domains. Energy-dispersive X-ray (EDX) cross-section analysis of the thin-film (Figure 1E) shows a contrast between Si Kα1 and Sn Lα1 signals and those associated with La Lα1, Fe Lα12 and Ti Kα1. The intensities maps suggest that the thickness of the LFO/TiO_2 film is in the range of 250 to 300 nm.

Figure 2A contrasts cyclic voltammograms (CV) of as-deposited LFO films and after various modifications recorded at 50 mVs^{-1} in Ar-saturated electrolyte solution containing 0.1M Na_2SO_4 at pH 12 in the dark. The LFO electrode shows a small capacitive current of the order of 1×10^{-6} A cm^{-2} across a large potential range, with a noticeable broadening at potentials above 1.2 V, suggesting interfacial hole accumulation. Indeed, we have constructed a Mott-Schottky plot (Figure S1) from electrochemical impedance data, showing the characteristic p-type behavior and a flatband potential close to 1.44 V vs. RHE. This value is consistent with the recent report by Choi and co-workers on LFO thin films.[16] A doping density of the order of 6×10^{17} cm^{-3} can be estimated from the slope of the Mott-Schottky, although this value should be considered with caution. On the one hand, we have used the geometric surface area which may significantly overestimate the density of acceptor states. On the other hand, there is also uncertainty in the relative permittivity of ferrites which are rather large (of the order of 10^4) and strongly dependent on the material structure.[21] As the interface going into accumulation regime, the onset of the oxygen evolution reaction (OER) can be observed close to 1.5 V.

Deposition of Pt nanoparticles (LFO/Pt, maximum loading of 0.19 mg cm^{-2}) leads to an increase of the capacitance across the whole potential range. By contrast, the capacitive current marginally increases upon deposition of TiO_2 thin film onto LFO (LFO/TiO_2), which promotes interfacial charge accumulation at potentials more negative than 0.6 V. The CV of a TiO_2 film deposited onto the FTO electrode (labelled as TiO_2 in Figure 2A) shows similar responses to the LFO/TiO_2 films but displaced by approximately 200 mV toward more negative potentials. As illustrated in Figure 2B, the shift in the onset potential for electron accumulation in the TiO_2 layer is a manifestation of the built-in potential generated upon equilibrating the Fermi levels at the LFO/TiO_2 heterojunctions. As the TiO_2 annealing was restricted to 500°C, we expect a rather abrupt junction at LFO/anatase nanoscale domains with very little elemental interdiffusion. As the junction is formed, we predict a shift of approximately 0.2 V in the conduction band edge of TiO_2 toward more positive potentials (Figure 2B), which is consistent with the shifts in the onset of electron accumulation of TiO_2 on FTO with respect to LFO (Figure 2A). This case is expected to be rather different from epitaxial LFO films grown by pulsed laser deposition onto single-crystalline $SrTiO_3$ surfaces.[22] A slight shift of valance band edge position of LFO onwards more negative potentials is also expected, however, the main effect seen upon the formation of the LFO/TiO_2 junction is the suppression of the OER at positive potential. Features associated with carrier accumulation are less evident in the case of LFO/TiO_2/Pt heterostructure, due to the increase in the capacitance across the entire potential range introduced by the metallic domains.

Figure 2C contrasts cyclic voltammograms of LFO and LFO/TiO_2 constructs at 5 mV s^{-1} in Ar-saturated 0.1M Na_2SO_4 aqueous solution at pH 12 under a square wave light perturbation at 464 nm. Photocurrent responses associated with HER are clearly seen across the potential window, with a significantly larger amplitude in the case of LFO/TiO_2. These results bring about two interesting observations: (1) the deposition of an insulating layer leads to an increase of the cathodic photocurrent responses across the entire potential range and (2) the photocurrent onset potential is shifted to values as positive as 1.47 V vs. RHE. Based on the proposed band alignment in Figure 2B, the conduction band of TiO_2 is estimated to be about 0.78 eV below the conduction band and 1.78 eV above the valence band of LFO. Consequently, TiO_2 can effectively block the OER mediated by holes in the valence band of LFO, while photogenerated electrons can be transported via the conduction band of TiO_2. This mechanism is different from the trap-mediated transport observed in TiO_2 protected photoanodes.[23]

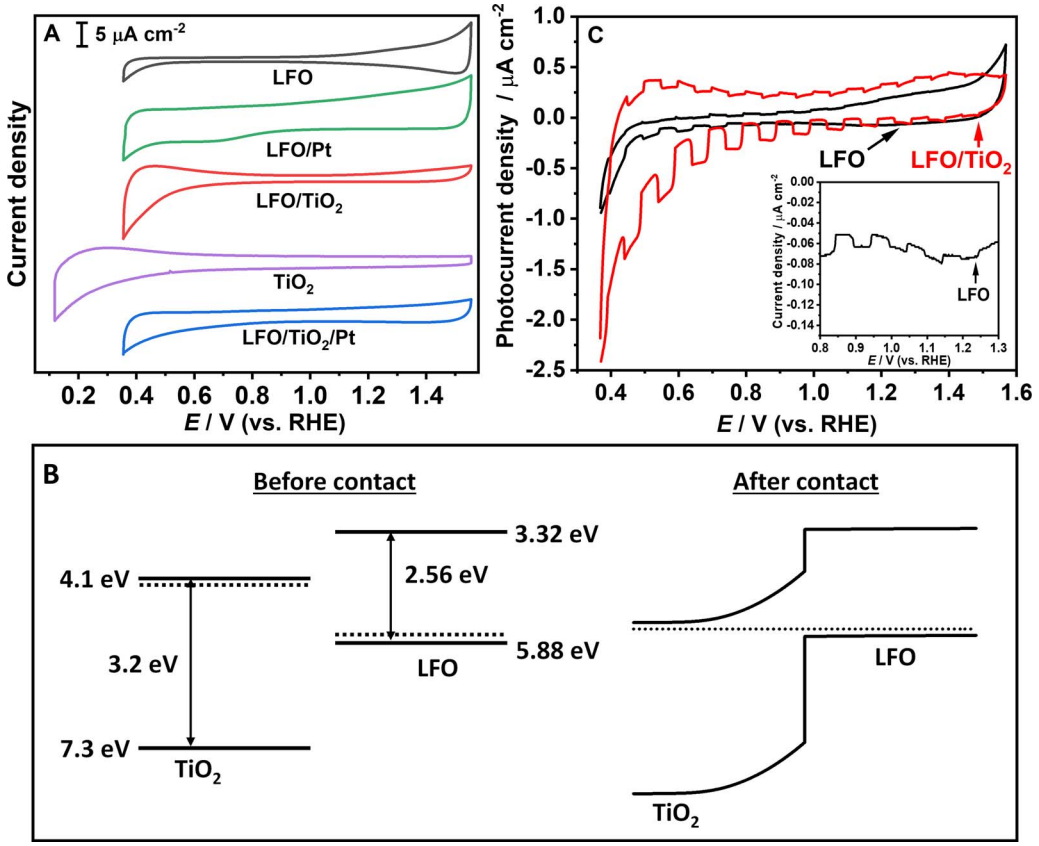

Figure 2. Electrochemical and photoelectrochemical responses of the nanostructured LFO based electrodes: cyclic voltammograms of the various constructs in Ar-purged aqueous solution containing 0.1 M Na_2SO_4 at pH 12; Estimation of the band alignment of LFO and TiO_2 prior and after the formation of the heterojunction, based on the Mott-Schottky plots shown in Figure S1 and majority carrier density of the order of 10^{17} cm^{-3} in the TiO_2 film (B); Cycling voltammogram of LFO and LFO/TiO_2 under the illumination at 464 nm and photon flux of 2.17×10^{15} cm^{-2} s^{-1} (C). Arrows indicates the position of photocurrent onset potential, while the inset shows the current responses of LFO electrodes at the positive end of the potential window.

Further information about the transport of photogenerated electron across the TiO_2 layer can be obtained from assessing the effect of the number of TiO_2 coating steps. Figure S2A contrast cyclic voltammograms of $Fe(CN)_6^{4-}$ at FTO electrodes modified by one to three TiO_2 coating steps. Each deposition step is followed by drying at 225 °C (5 min) and annealing at 500 °C (30 min). The voltammograms in Figure S2A show an increase in the peak-to-peak separation after the first two deposition steps, while a significant drop in the current is observed after 3 deposition steps. Semi-quantitative analysis of the voltammetric responses employing the Nicholson-Shain formalism shows that the phenomenological charge transfer rate constant decreases by 40 times between 1 and 3 deposition coatings (Table S1). Employing the partially blocked electrode model,[24–26] we estimate that the TiO_2 coverage increases from 72.5% to 97.5% from 1 to 3 coating steps. Interestingly, the dependence of the photocurrent responses on the number of coating steps is rather small as shown in Figure S2B. A significant *increase* in the current is observed upon adsorbing the first TiO_2 layer, while less than 20% fall of the photocurrent is observed at negative potentials upon increasing the number of TiO_2 coating steps. This observation reveals that the coverage and thickness of the TiO_2 layer have little influence on the transport of photogenerated electrons. This is not surprising given that the LFO conduction band edge is located well above the one of TiO_2 (see Figure 2), carrier transport to the surface occurs by the conduction band of the nanostructured TiO_2 layer. It can be anticipated that this process would manifest itself by the characteristic spectroscopic features of electrons in the TiO_2 conduction band which could be approached by time-resolved spectroscopy.

The external quantum efficiency (EQE) at 0.5 V at various wavelengths is shown in Figure 3A, which can be contrasted with the optical responses of LFO films as probed by the diffuse reflectance spectra of the films in Figure 3B. Analysis of the transmission and reflectance spectra based on Tauc plot (Figure 3C) show two distinctive transitions similar to those reported in epitaxially grown $LaFeO_3$ films.[27] Indeed, optical transitions in $LaFeO_3$ are complex due to multiple interband transitions involving majority and minority spin-states arising from the octahedral splitting of Fe 3d in t_2g and eg levels, respectively.[27] The features of the tauc plot in Figure 3C are closely reproduced by equivalent plots constructed from the EQE spectra of the various photoelectrode constructs (supplemental material, Figure S3). This close correlation between optical and photoelectrochemical responses demonstrates that carriers are generated and collected across the LFO spectral range with a fundamental bandgap at 2.56 eV. We also observe some tailing in the optical and photoelectrochemical responses beyond the bandgap which can be associated with structural disorder in the nanostructured absorber layer.

Photocurrent transient responses for the various thin-film constructs recorded under 10 s illumination at 464 nm and different applied potentials are contrasted in Figure 3D. The deposition of Pt onto the LFO films only leads to small increases in the photoresponses with respect to the as-deposited LFO electrodes. It can also be seen that the photocurrent rise time in the light on-transient and the relaxation in the off-transient are significantly slower at negative potentials. As described by Zhang et al.,[28] this behavior can be rationalized in terms of trap-limited transport of majority carriers. At negative potentials, trap-states are filled with electrons, slowing down the transport of holes to the back contact through the network of LFO nanoparticles. The photocurrent in the presence of TiO_2 film increases across the whole potential range while the photocurrent at the LFO/TiO_2/Pt construct shows the largest improvement in the photocurrent. The transient responses show a noticeable decrease after the initial response upon

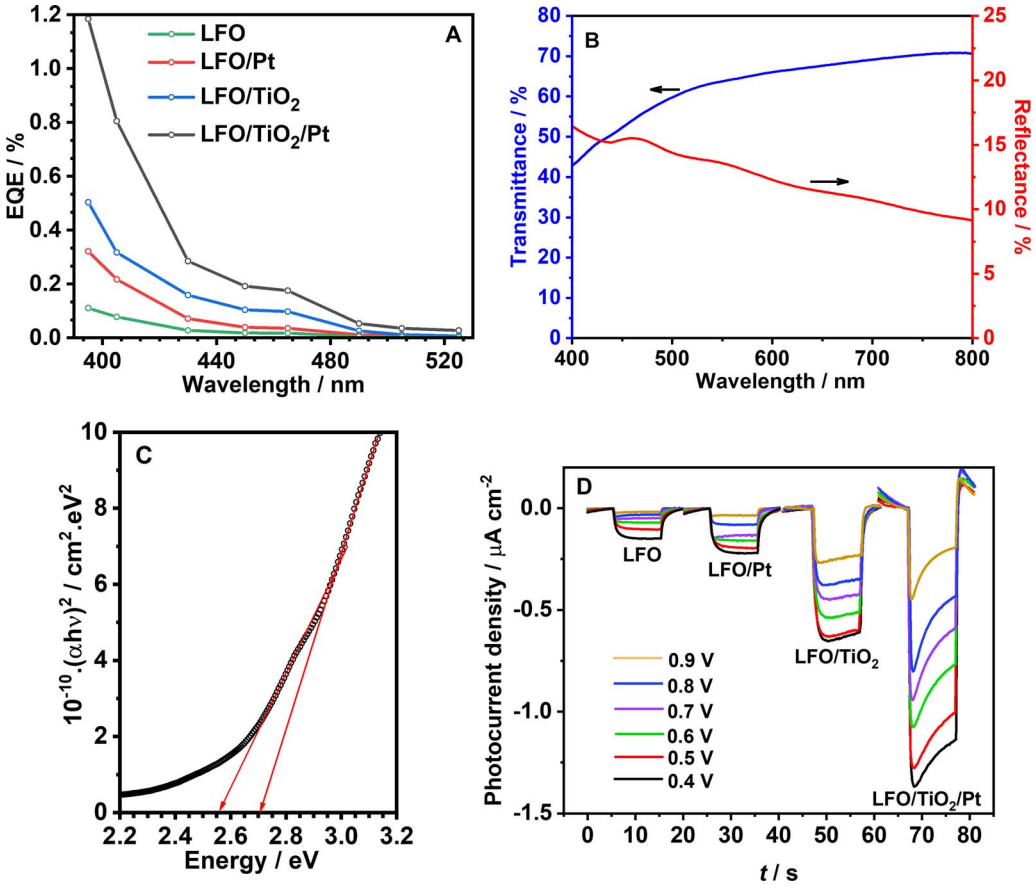

Figure 3. Photoelectrochemical and optical responses of the various photoelectrode constructs: external quantum efficiency (EQE) spectra at 0.5 V vs. RHE in Ar-saturated 0.1M Na_2SO_4 aqueous solution at pH 12 (A). Diffuse reflectance and transmittance spectrum of LFO film (B) and Tauc plot analysis (C) revealing two edges separated by approximately 150 meV (C). Photocurrent transient measurements of the various photocathodes at different potentials in Ar-saturated 0.1M Na_2SO_4 aqueous solution (pH 12) and a photon flux of 3.44×10^{15} cm^{-2} s^{-1} (D).

illumination, with a positive photocurrent overshoot in the off-transient. These responses provide evidence of surface recombination reactions, which are not apparent in the absence of the TiO_2 film. Varying the Pt loading via the number of coating steps from 0.19 mg cm^{-2} to 0.76 mg cm^{-2}, the photocurrent responses exhibit a maximum value at 0.38 mg cm^{-2} (see supplemental material, Figure S4).

Our findings offer an approach to improve the performance of these interesting and electrochemically robust materials. TiO_2 act as a hole-blocking layer increasing their collection efficiency at the back contact, while Pt nanostructures facilitate the HER reaction at the surface of the construct. Although evidence of surface recombination can be seen in the photoelectrochemical responses of LFO/TiO_2 heterostructures, bulk recombination remains the dominant carrier-loss pathway. Indeed, Figure S5 contrasts external and internal quantum efficiencies (IQE) spectra of LFO films, based on their reflectance and transmission spectra. The IQE is approximately three times larger than EQE across the whole visible spectrum, which further confirms the challenges associated with bulk recombination in this material. In this context, grain boundaries in the nanostructured films may represent a strong barrier to hole transport, given the tendency of La to segregate to the surface in the thermolysis of these type of precursors.[17,29,30] Consequently, improvement in EQE can be promoted by substantially increasing crystalline domains in LFO, as well as further optimization of the TiO_2 film thickness and HER catalysts size and loading.

Conclusions

Sequential deposition of TiO_2 thin films and Pt nanoparticles onto nanostructured LFO thin films employing entirely solution-based methods leads to a 10-fold increase in the photoelectrochemical responses toward the hydrogen evolution reaction. EQE values above 1% at 400 nm were recorded in alkaline solution (pH 12) at 0.5 V. Integrating the EQE spectral response provides photocurrent responses up to 0.015 mA cm^{-2} under AM 1.5 illumination. However, the most striking observation of these constructs is the photocurrent onset potential close to 1.5 V vs. RHE, which is the most positive value recorded for a single absorber photoelectrode. The TiO_2 layer acts as a barrier for hole transfer to the electrolyte, suppressing dark current and the loss of majority carriers (via water oxidation). The formation of a heterojunction at the LFO/TiO_2 interface is demonstrated by a positive shift in the onset potential of electron accumulation in the TiO_2 layer in the dark. These studies show the potential for this class of material to act as photocathode in sustainable integrated photoelectrochemical water-splitting. However, there are significant carrier losses in these systems which are dominated by bulk recombination in the nanostructured absorber layer.

Acknowledgments

XS is indebted to the School of Chemistry of the University of Bristol for enabling sponsoring access to research facilities. DT is thankful to the Engineering and Physical Sciences Research Council for funding through the University of Bristol Impact Acceleration Account.

ORCID

David J. Fermin https://orcid.org/0000-0002-0376-5506

References

1. J. H. Montoya, L. C. Seitz, P. Chakthranont, A. Vojvodic, T. F. Jaramillo, and J. K. Nørskov, *Nat. Mater.*, **16**, 70 (2016).
2. J. L. Young, M. A. Steiner, H. Döscher, R. M. France, J. A. Turner, and T. G. Deutsch, *Nat. Energy*, **2**, 17028 (2017).
3. D. Kang, J. L. Young, H. Lim, W. E. Klein, H. Chen, Y. Xi, B. Gai, T. G. Deutsch, and J. Yoon, *Nat. Energy*, **2**, 17043 (2017).
4. M. M. May, H. J. Lewerenz, D. Lackner, F. Dimroth, and T. Hannappel, *Nat. Commun.*, **6**, 8286 (2015).
5. S. Hu, M. R. Shaner, J. A. Beardslee, M. Lichterman, B. S. Brunschwig, and N. S. Lewis, *Science*, **45**, 1005 (2014).
6. E. Verlage, S. Hu, R. Liu, R. J. R. Jones, K. Sun, C. Xiang, N. S. Lewis, and H. A. Atwater, *Energy Environ. Sci.*, **8**, 3166 (2015).
7. M. G. Walter, E. L. Warren, J. R. McKone, S. W. Boettcher, Q. Mi, E. A. Santori, and N. S. Lewis, *Chem. Rev.*, **110**, 6446 (2010).
8. K. Rajeshwar, M. K. Hossain, R. T. Macaluso, C. Janáky, A. Varga, and P. J. Kulesza, *J. Electrochem. Soc.*, **165**, H3192 (2018).
9. J. Luo, L. Steier, M. K. Son, M. Schreier, M. T. Mayer, and M. Grätzel, *Nano Lett.*, **16**, 1848 (2016).
10. M. I. Díez-García and R. Gómez, *ACS Appl. Mater. Interfaces*, **8**, 21387 (2016).
11. M. S. Prévot, N. Guijarro, and K. Sivula, *ChemSusChem*, **8**, 1359 (2015).
12. V. Celorrio, K. Bradley, O. J. Weber, S. R. Hall, and D. J. Fermín, *ChemElectroChem*, **1**, 1667 (2014).
13. G. S. Pawar and A. A. Tahir, *Sci. Rep.*, **8**, 3501 (2018).
14. G. P. Wheeler and K. S. Choi, *ACS Energy Lett.*, **2**, 2378 (2017).
15. M. I. Díez-García and R. Gómez, *ChemSusChem*, **10**, 2457 (2017).
16. G. P. Wheeler, V. U. Baltazar, T. J. Smart, A. Radmilovic, Y. Ping, and K.-S. Choi, *Chem. Mater.*, **31**, 5890 (2019).
17. V. Celorrio, L. Calvillo, E. Dann, G. Granozzi, A. Aguadero, D. Kramer, A. E. Russell, and D. J. Fermín, *Catal. Sci. Technol.*, **6**, 7231 (2016).
18. M. I. Díez-García, V. Celorrio, L. Calvillo, D. Tiwari, R. Gómez, and D. J. Fermín, *Electrochim. Acta*, **246**, 365 (2017).
19. V. Celorrio, E. Dann, L. Calvillo, D. J. Morgan, S. R. Hall, and D. J. Fermin, *ChemElectroChem*, **3**, 283 (2016).
20. C. C. Leuw, S. T. Chen, and F. K. Liu, *J. Am. Ceram. Soc.*, **93**, 3142 (2010).
21. S. Acharya, J. Mondal, S. Ghosh, S. K. Roy, and P. K. Chakrabarti, *Mater. Lett.*, **64**, 415 (2010).
22. K. J. May, D. P. Fenning, T. Ming, W. T. Hong, D. Lee, K. A. Stoerzinger, M. D. Biegalski, A. M. Kolpak, and Y. Shao-Horn, *J. Phys. Chem. Lett.*, **6**, 977 (2015).
23. P. Nunez, M. H. Richter, B. D. Piercy, C. W. Roske, M. Cabán-Acevedo, M. D. Losego, S. J. Konezny, D. J. Fermin, S. Hu, B. S. Brunschwig, and N. S. Lewis, *J. Phys. Chem. C*, **123**, 20116 (2019).
24. J. Zhao, C. R. Bradbury, and D. J. Fermín, *J. Phys. Chem. C*, **112**, 6832 (2008).
25. C. Amatore, J. M. Savéant, and D. Tessier, *J. Electroanal. Chem.*, **147**, 39 (1983).
26. C. R. Bradbury, J. Zhao, and D. J. Fermín, *J. Phys. Chem. C*, **112**, 10153 (2008).
27. M. D. Scafetta, Y. J. Xie, M. Torres, J. E. Spanier, and S. J. May, *Appl. Phys. Lett.*, **102**, 081904 (2013).
28. Q. Zhang, V. Celorrio, K. Bradley, F. Eisner, D. Cherns, W. Yan, and D. J. Fermín, *J. Phys. Chem. C*, **118**, 18207 (2014).
29. V. Celorrio, L. Calvillo, C. A. M. van den Bosch, G. Granozzi, A. Aguadero, A. E. Russell, and D. J. Fermín, *ChemElectroChem*, **5**, 3044 (2018).
30. V. Celorrio, L. Calvillo, G. Granozzi, A. E. Russell, and D. J. Fermin, *Top. Catal.*, **61**, 154 (2018).